J. Fluid Mech. (1965), *vol.* 21, *part* 4, *pp.* 673–688
Printed in Great Britain

Thermal conductivity of argon at high temperatures

By MORTON CAMAC AND ROBERT M. FEINBERG
Avco-Everett Research Laboratory, Everett, Massachusetts

(Received 6 July 1964)

An infra-red heat-transfer gauge was used in a shock tube for end-wall measurements of the convective heat transfer from argon behind the reflected shock. The thermal conductivity of neutral (un-ionized) argon was measured before the ionization-relaxation time, and was fitted with the power-law temperature dependence $4{\cdot}2 \times 10^{-5}(T/300)^{0{\cdot}76\pm0{\cdot}03}$ cal/sec cm °K, where T is measured in °K, and $\pm 0{\cdot}03$ refers to the probable error. The free-stream temperature ranged from 20,000 to 75,000 °K, corresponding to incident-shock velocities from 3 to 6 mm/μsec. At later times, after the free stream established equilibrium ionization, the convective-heat-transfer rate remained the same as the initial rate with neutral argon. Theoretical predictions of Fay & Kemp (1965), assuming equilibrium-boundary-layer conditions, are 20–30 % below the experimental values. Also reported in this paper are measurements of the ionization times behind the reflected shock, and these are in agreement with an extrapolation of the Petschek & Byron (1957) measurements behind the incident shock. There is a discussion of the large changes in the gas conditions behind the reflected shock due to the ionization process. The final equilibrium conditions are reached abruptly, as indicated by the continuum-radiation emission which becomes constant immediately after ionization relaxation.

1. Introduction

The interaction of a hot, ionized plasma with a cold wall is of interest in several fields. Examples are plasma arcs, plasma propulsion motors, high-speed flight in re-entry, and many fusion machines. Critical to the evaluation of the thermal losses to the walls is the knowledge of both the transport properties of the plasma and the effects of recombination chemistry in the vicinity of the colder walls. This paper reports on an experimental study of the heat transfer from high-temperature argon to the shock-tube end-wall. Argon was chosen because its transport properties (Fay 1964; Amdur & Mason 1958) and chemical kinetics (Petschek & Byron 1957; Petschek *et al.* 1955) have been extensively studied. This permits a theoretical comparison with the experimental data, and thus, a check on the understanding of heat conduction from high-temperature gases to surfaces.

There have been several experimental studies of the heat transfer from argon. Van der Noordaa (1957) measured the heat-transfer rates on the side wall of the shock tube behind the incident shock. Bershader & Rutowski (1961) and Reilly (1963) measured the stagnation-point heat transfer on a hemispherical

body. Measurements of the end-wall heat transfer for temperatures to 4000 °K were reported by Smiley (1957) and Sturtevant (1964). In the present paper, measurements were extended to 75,000 °K in neutral argon, and up to 55 % ionization after gas equilibration.

A general theory for the heat transfer from argon (Jukes 1956) has been applied to the end-wall boundary layer by Camac & Kemp (1963), but no results are reported. They considered non-equilibrium chemistry using the known ionic recombination rates, and different electron and heavy-particle temperatures due to the weak thermal coupling between these species. The electron temperature remains high throughout the boundary layer, because the sheath potential at the wall essentially insulates electrons from the wall.

A more restricted theoretical analysis has been reported by Fay & Kemp (1965). They evaluated the end-wall heat-transfer from argon for two cases: (i) frozen (no gas-phase recombination) boundary-layer chemistry, and (ii) complete chemical equilibrium. For these limiting conditions, all species have the same temperature for our conditions. Our experimental results are compared to their work in the final section.

The paper consists of four sections. The next section discusses the factors that determine the argon conditions behind the reflected shock both for the free stream and the boundary layer. These properties were used in the companion paper (Fay & Kemp 1965) in their evaluation of the end-wall heat-transfer rates. An experimental section follows, describing measurements of the argon heat-transfer rates to the end-wall and ionization times behind the reflected shock. In the final section, the experimental data will be summarized and compared to the theoretical predictions.

2. Theory

The theoretical evaluation of the end-wall heat-transfer rates requires a knowledge of (i) the gas conditions behind the reflected shock, and (ii) the transport properties and chemical kinetics of argon in the boundary layer. The first item is outlined in this section and presented in more detail in Camac & Feinberg (1963). The boundary-layer phenomena are treated in the companion paper (Fay & Kemp 1965). The free-stream gas conditions are mainly determined by the steady-state reflected-shock solutions for neutral argon and for equilibrium ionization. Other effects that must be evaluated are the unsteady flow field due to the ionization process and end-wall cooling, the rate of ionization of argon, and gas cooling by the intense continuum radiation.

2.1. *Gas conditions behind the reflected shock*

A variety of free stream conditions has been identified by our end-wall measurements, and they are illustrated in figure 1. This is a schematic (x,t)-diagram at the end-wall showing the incident and reflected shocks, each followed by a frozen region and an ionization front after time intervals τ_2 and τ_4 respectively. It should be noted that initially the reflected shock velocity is that for frozen argon, i.e. for constant $\gamma = \frac{5}{3}$. However, when most of the gas behind the reflected

shock is ionized, then the reflected-shock velocity decreases to that for equilibrium ionization behind the shock. Furthermore, the gas behind the incident shock may be either frozen or in equilibrium. These various regions are indicated in figure 1 by the symbols 2F–4F, 2F–4E and 2E–4E, indicating where regions 2 (behind the incident shock) and 4 (behind the reflected shock) are frozen F, or in equilibrium E. At the start of the ionization process, the flow becomes unsteady because of the strong interaction of the ionization process with the flow field. The gas conditions at the wall just after ionization has taken place, designated by 2F–4E′ in figure 1, have been estimated (Camac & Teare 1964) for this unsteady flow and will be discussed later.

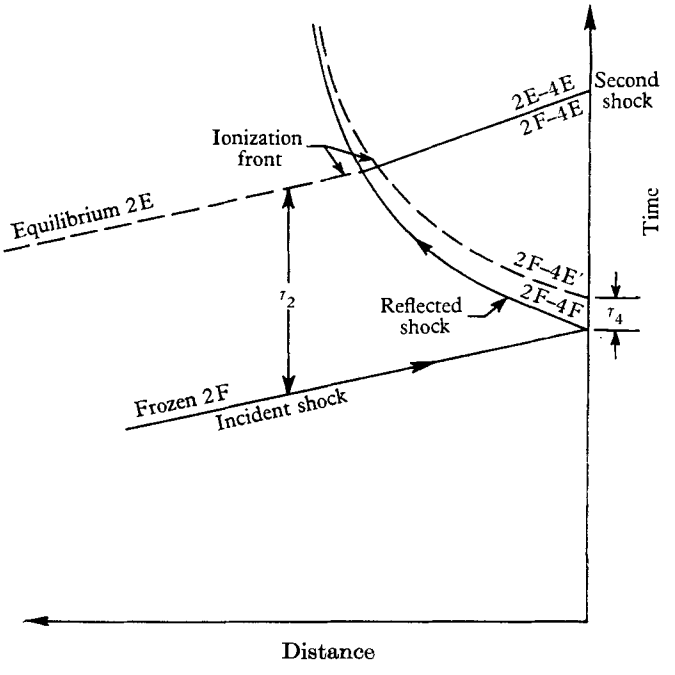

FIGURE 1. Schematic (x,t)-diagram at the end-wall showing the incident and reflected shocks, each followed by a frozen region and an ionization front. End-wall heat-transfer measurements were obtained from region 2F–4F to region 2E–4E. τ_4 was also measured.

The state of the shock-heated argon for the cases of no ionization (frozen conditions) and equilibrium ionization can be determined directly from the steady-state flow equations across the incident and reflected shocks (Camac & Feinberg 1963). These conditions are presented in table 1 for our experimental range of shock-velocities (from 3 to 6 mm/μsec), for an initial argon pressure of 1 mm Hg and temperature of 294 °K. Note the large changes in the conditions (e.g. the change from region 2F–4F to 2F–4E has up to a factor of 5 drop in the temperature).

The change in conditions across the ionization front is so drastic that this transition itself becomes an interesting process to analyse (Camac & Teare 1964). Near the wall, the gas essentially at rest in the frozen region behind the reflected shock is set in motion toward the wall by the large pressure change across the

ionization front. A complicated wave pattern results, stopping the gas at the wall again. These waves also propagate to the reflected shock, causing a reduction in its velocity. To evaluate the free-stream conditions at the end-wall as functions of time, all these waves produced by the chemistry would have to be considered.

A simplified version of this flow field was assumed in Camac & Teare (1964), from which the conditions after ionization could be estimated. The basic assumption was that the argon chemistry remained *frozen* until the ionization time, and then abruptly went to equilibrium. This assumption of an abrupt ionization process was suggested by the sudden onset of continuum radiation behind the reflected shock after the predicted ionization time τ_4 (see figure 9, plate 1).

Incident-shock velocity	Density (ρ/ρ_1)			Temperature (°K)			Degree of ionization (α)	
(mm/μsec)	2F–4F	2F–4E	2E–4E	2F–4F	2F–4E	2E–4E	2F–4E	2E–4E
3	9·55	13·50	14·30	19,500	11,100	11,200	0·069	0·072
4	9·73	18·10	28·00	34,500	12,700	13,350	0·175	0·206
5	9·82	22·10	45·50	54,000	14,100	15,400	0·318	0·385
6	9·87	25·35	62·00	78,000	15,500	17,500	0·490	0·600

TABLE 1. Argon conditions behind the reflected shock.

Incident-shock velocity	Density (ρ/ρ_1)		Temperature (°K)		Pressure (p/p_1)		Degree of ionization (α)		Radiation intensity $(\alpha)^2(\rho/\rho_1)^2/\sqrt{T}$	
(mm/μsec)	2F–4E′	2F–4E	2F–4E′	2F–4E	2F–4E′	2F–4E	2F–4E′	2F–4E	2F–4E′	2F–4E
3	13·0	13·6	11,300	11,100	542	560	0·08	0·07	0·010	0·009
4	16·9	18·1	12,900	12,700	900	930	0·21	0·18	0·111	0·094
5	20·3	22·1	14,400	14,100	1354	1400	0·37	0·32	0·470	0·421
6	22·8	25·3	15,800	15,500	1912	1980	0·56	0·49	1·30	1·23

TABLE 2. Comparison of conditions at end-wall behind expansion fan* (region 2F–4E′) with that for equilibrium (region 2F–4E).

* Data taken from Camac & Teare (1964).

Table 2 shows a comparison of the gas conditions at the end-wall behind the ionization front (region 2F–4E′) with the conditions at equilibrium (region 2F–4E). Note that the conditions vary by only a few percent. Also, the continuum radiation emission, which is proportional to $[(\rho/\rho_1)^2\alpha^2T^{-\frac{1}{2}}]$, does not vary. A constant visible-light emission is observed (see the linear slope in figure 9).

The transition from the region 2F–4E to 2E–4E is also interesting. The interaction between the reflected shock and the large change in the gas density during ionization in region 2 produces a disturbance, probably a shock wave, which propagates to the end-wall. The effect is observed in our experiment by a discontinuity in the heat-transfer rate at the end-wall and in the visible light emission behind the reflected shock (see figures 5 and 9 plate 1).

2.2. *Argon ionization times*

The curves in figure 7 show the argon ionization times behind the incident shock, τ_2 (Petschek & Byron 1957) and the reflected shock, τ_4, as a function of the incident-shock velocity for an initial argon pressure of 1 mm Hg. τ_4 was obtained by extrapolating the experimental data of Petschek & Byron (1957), whose result for the ionization (laboratory) time behind the incident shock is

$$\tau_2 = (0{\cdot}156/p_1)\exp(87{,}000/T_2)\,\mu\text{sec}. \tag{1}$$

p_1 is the initial argon pressure in mm Hg, and T_2 is the frozen (no ionization) temperature behind the incident shock in °K. This formula is extrapolated to the conditions behind the reflected shock by the relation

$$\tau_4 = (0{\cdot}156/p_1)(\rho_2/\rho_1)(\rho_2/\rho_4)\exp(87{,}000/T_4)\,\mu\text{sec}. \tag{2}$$

T_4 is the frozen temperature behind the reflected shock; (ρ_2/ρ_1) and (ρ_4/ρ_2) are the frozen density ratios across the incident and reflected shocks respectively. The factor (ρ_2/ρ_1) transforms equation (1) to particle time; (ρ_2/ρ_4) and T_4 correct for the density and temperature conditions behind the reflected shock. Note the ionization time behind the reflected shock is less than for the incident shock; thus, the gas conditions at the end-wall remain frozen until τ_4, as illustrated in figure 1. In § 3, we present measurements of τ_4 which are in agreement with equation (2).

2.3. *Radiation cooling*

After the argon reaches equilibrium ionization, the continuous radiative emission can cause an appreciable reduction of the gas enthalpy. Two effects must be evaluated for possible corrections to the heat-transfer experiment: (i) radiation cooling of the free-stream gas, and (ii) the radiative heat transfer to the gauge. When only the convective component of the heat transfer is desired, the radiative-heat-transfer effects must be suppressed, or at least subtracted away. As will be shown in § 3, the high-reflectivity-aluminium-gauge surface and the unsteady flow at the end-wall permit a separation of the radiative and convective heating.

The argon radiation intensity per unit volume has been determined by Petschek *et al.* (1955) and by Mies (1962). The radiation cooling times for the equilibrium conditions behind the incident and the reflected shocks are plotted as a function of the incident-shock velocity in figure 2. For region 2F–4E and shock velocities below 5 mm/μsec, the radiation cooling times are long (in excess of 100 μsec). At the higher shock velocities, the heat-transfer measurements were made within 3 μsec, and the gas enthalpy loss through radiation does not exceed 3 %. For regions 2E–4E, the cooling times are much shorter and become an important loss term. In addition, corrections for the effects of radiative heat transfer to the gauge must be included (see figure 5).

2.4. *Effect of end-wall cooling*

Goldsworthy (1959) evaluated the effects of the end-wall thermal boundary layer on the free stream behind the reflected shock. This theory was experimentally verified by Sturtevant (1964). The boundary layer gives rise to a negative dis-

placement thickness, which causes the gas behind the reflected shock to flow toward the end-wall, which, in turn, reduces the reflected-shock velocity from that with no wall cooling. For our experimental conditions of a 1 mm initial argon pressure, the variation of the reflected-shock velocity u'_{RS} with time becomes

$$u'_{RS} = u_{RS}\{1 - \sqrt{(0{\cdot}016/t)}\}, \tag{3}$$

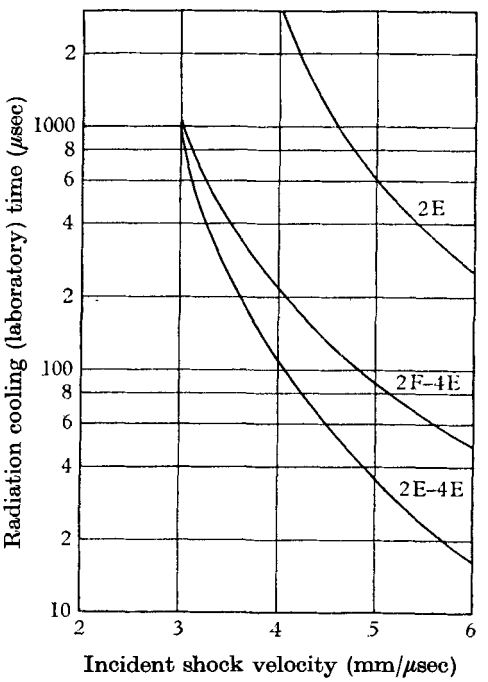

FIGURE 2. Radiation cooling times behind the incident and reflected shocks in argon with an initial pressure of 1 mm Hg and temperature of 294° K. Regions 2E, 2F–4E and 2E–4E are indicated in figure 1.

where u_{RS} is the reflected-shock velocity with no boundary layer, and t is measured in μsec. It should be noted that after 1 μsec, where most of our experimental measurements start, the correction to the shock velocity is 10 %. This flow and the resulting changes in the gas conditions were neglected in the theoretical evaluation of the end-wall heat transfer.

Another boundary-layer interaction was reported (Byron & Rott 1961), but has no effect on our experimental measurements. The interaction of the reflected shock with the side-wall boundary layer behind the incident shock leads to separated flow in some cases, which, in turn, affects the gas conditions behind the reflected shock. For argon with low degrees of ionization, there is no separated flow, and the effect on the free stream is unimportant. For high degrees of ionization, our heat-transfer measurements are made shortly after the onset of the reflected shock and before the side-wall boundary-layer interactions can affect the free-stream conditions in the vicinity of the heat-transfer gauge, i.e. at the centre of the shock tube.

2.5. *End-wall boundary layer properties*

The end-wall boundary layer using the gas sample behind the reflected shock is essentially a Rayleigh problem. A gas sample at rest with respect to the wall is abruptly raised to a high temperature. There is only a thermal boundary layer, whose properties depend on the concentration, thermal conductivity, and diffusion rate of each species. Effects of viscosity do not appear, because there is no flow parallel to the wall. This permits a simplification of the boundary-layer theory.

The major disadvantage to the end-wall geometry is that the boundary layer grows with time, and there is no steady state. During this time, the external gas conditions have large changes which further complicate the evaluation of the chemical state of the boundary layer. Initially, the free-stream argon is frozen at a high temperature with no ionization. The ionization process is slower in the boundary layer than in the free stream; *the boundary layer remains frozen until the free-stream ionization time* τ_4. Thus, the end-wall heat transfer prior to τ_4 is due to neutral argon.

The ionization process in the free stream occurs rather abruptly, and the free-stream temperature drops below that for part of the boundary layer, causing rapid boundary-layer cooling to both the end wall and the free stream in a time that is short compared to τ_4. During this time, the ionization in the boundary layer is negligible, and electrons must diffuse into the boundary layer from the free stream.

For sufficiently long times compared to τ_4, the effects of the finite rate for the free-stream ionization become negligible, and it is reasonable to assume that equilibrium free-stream conditions existed back to the time of the formation of the boundary layer. With this assumption, similarity solutions for the boundary layer were obtained by Fay & Kemp (1965) for the two limiting cases: (i) no gas-phase recombination (frozen chemistry), and (ii) complete ionization equilibrium in the boundary layer. Our experimental data are compared to their results in figure 8. These limiting cases do not bracket the general solution which would allow for different electron and heavy particle temperatures. It can be shown (Camac & Feinberg 1963) that the equilibrium boundary solution is closer to our experimental conditions.

3. Experiments

This section contains a description of the experimental apparatus and the measurements. The features of the infra-red-heat-transfer gauge are first discussed. Two series of measurements were performed from which the following properties of shock-heated argon were obtained: (i) the convective heat transfer to the end-wall, and (ii) the time to reach ionization equilibrium.

3.1. *Infra-red-heat-transfer gauge*

Figure 3 shows the components of the heat-transfer system. The requirements for the gauge, the optical system, and the infra-red detector are reported elsewhere (Camac & Feinberg 1962). A portion of the shock-tube end-wall is replaced

with a $\frac{3}{8}$ in. diameter, 0·019 in. thick, sapphire window coated with a thin layer of carbon, and overcoated with aluminium. Infra-red radiation from the gauge is imaged with mirrors on a 2 mm by 2 mm gold-doped-germanium infra-red cell. Convective and radiative heating from the shock-heated argon is applied on the aluminium-coated side of the opaque layer, and changes in temperature are determined from measurements of the (essentially black body) infra-red emission from the back side of the carbon. Since the layer is initially at room temperature,

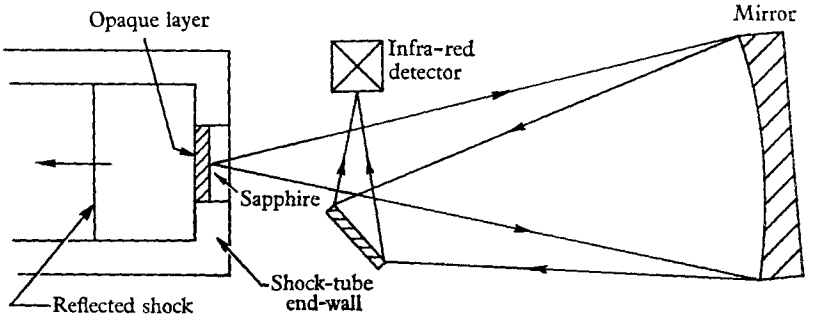

FIGURE 3. Experimental arrangement for the end-wall heat-transfer measurements.

the predominant radiation is in the infra-red band from 5 to 30 μ. The opaque layer is made thin enough so the temperature of the front surface can be determined in less than 0·1 μsec (see figure 9). All effects from the plasma, except thermal and radiative heating, are isolated from the infra-red detector by the opaque layer. There is no problem with electric shorting or photo-electric pick-up which affect resistance-type gauges. Radiative heating of the gauge is reduced considerably by the highly reflecting (emissivity less than 0·1) layer of aluminium, thereby permitting measurements of only the convective heat flux.

3.2. *Calibration of the heat-transfer-gauge system*

The output of the infra-red detector must be correlated to the heat fluxes to the heat-transfer gauge. The experimental set-up for calibrating the infra-red-heat-transfer gauge is essentially that for the shock-tube measurements except that the shock tube is replaced by a black body. A tank of well agitated, heated water in the range from 0 to 100 °C maintains a uniform temperature over the black-body cavity. A beam chopper placed in front of the source gives an a.c. method for calibrating the system; the emission from the surface of the chopper blade, when closed, serves as the reference level. The chopper frequency is of the order of 5000/sec. The output of the cell goes to a standard cathode follower and amplifier circuit, whose output is displayed on an oscilloscope.

The heat-transfer gauge in a shock-tube experiment receives a short heat pulse, and measurements are made within a few microseconds. Thus, the temperature of the opaque surface rises, while essentially all the sapphire remains at room temperature. It is impossible to match this situation directly in this static-calibration method, since the sapphire is also heated. However, the calibration for the short heat pulse can be evaluated by three series of measurements.

For the first measurement, a black-body source is imaged on the detector. The output of the infra-red detector V_1 is

$$V_1 = V_B - V_C, \tag{4}$$

where V_B is the signal due to the black body, and V_C is the signal due to the closed chopper wheel. It is important to note that V_C is also the signal from the black body when the black body is at the temperature of the chopper wheel.

In the second case, the same black-body source is used with the addition of a sapphire window, kept at room temperature, interposed between the black body and the chopper wheel. The detector output V_2 for this case is

$$V_2 = XV_B + (1-X)V_C - V_C = X(V_B - V_C). \tag{5}$$

X is the effective external transmission of the sapphire averaged over the spectral sensitivity of the Au:Ge detector (Camac & Feinberg 1962). The term XV_B is the attenuated contribution from the black body; $(1-X)V_C$ is the contribution from the sapphire. The effects of multiple reflexion from the sapphire surfaces are included.

In the third case, a heat-transfer gauge (the carbon layer on sapphire) in thermal contact with the black body is used for the source. Both the carbon and sapphire are kept at the temperature of the black body. The detector output V_3 is

$$V_3 = \left[\left(\frac{\epsilon X}{1-r}\right) + \left(1 - r - \frac{X}{1-r}\right)\right][V_B - V_C]. \tag{6}$$

ϵ is the carbon emissivity at the carbon-sapphire interface, and $r = 0{\cdot}08$ is the reflectivity at the sapphire-air surface. The term in the first parenthesis in equation (6) is the contribution from the carbon, while the second term is due to the radiation from the sapphire.

V_3 is the calibration of the system for long-time measurements, i.e. greater than seconds. For heat pulses of short duration, such as from shock-tube experiments, there is only the contribution from the first term in equation (6). There is no contribution from the second term, because essentially all of the sapphire remains at room temperature. The calibration signal, say V_G, for the short duration heat pulse becomes

$$V_G = \left(\frac{\epsilon X}{1-r}\right)(V_B - V_C) = \left(\frac{\epsilon}{1-r}\right) V_2. \tag{7}$$

In terms of the calibration measurements

$$V_G = V_2/(1-r) - (1-r)(V_1) + V_3. \tag{8}$$

Figure 4 shows the experimental calibration of the heat-transfer-gauge system. The detector output is plotted against the black-body temperature. The three curves labelled V_1, V_2 and V_3 correspond to the three cases just described. The response V_G of the gauge to a short heat pulse can be determined from these measurements with the use of equation (8). One finds that the emissivity of the carbon-sapphire interface is $\epsilon = 0{\cdot}95 \pm 0{\cdot}05$. Thus, the V_2 curve becomes a good approximation for V_G, because

$$V_G = \left(\frac{\epsilon}{1-r}\right) V_2 = \left(\frac{0{\cdot}95}{0{\cdot}92}\right) V_2 \approx V_2. \tag{9}$$

We found that it was more convenient and reliable to check the calibration of the heat-transfer system by periodically measuring the black-body calibration curve V_1. However, the heat-transfer experimental data must be compared to the calibration curve V_2. The ratio of V_2 to V_1 was measured quite accurately in a preliminary series of runs, and this ratio was used with the periodic checks of V_1 to obtain V_2 for calibration of the shock-tube measurements.

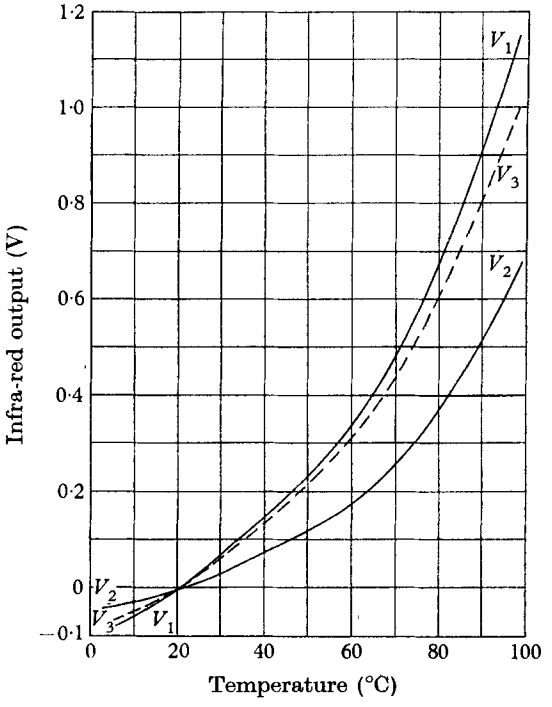

FIGURE 4. Heat-transfer-system calibration curves.

3.3. *Shock-tube measurements*

Measurements were made of the convective heat transfer to the shock-tube end-wall. The time for ionization of the argon behind the reflected shock was also measured in order to evaluate the chemical state during the heat-transfer observations. This information was used to determine the (x, t)-diagram shown in figure 1.

Measurements of end-wall heat transfer from the argon behind the reflected shock are shown in figure 5 (plate 1). These oscillograms show the infra-red-detector output as a function of time. The argon initial pressure was 1 mm Hg, and the incident-shock velocities were 4·60 and 4·97 mm/μsec. The sweep speeds for the two sets of traces are indicated in the figure. The signals show a sharp rise when the incident shock arrives at the end-wall, a flat portion representing convective heating, another rise to a second plateau, and then a further gradual rise.

Before analysing the heat-transfer experimental results, it is instructive to discuss the properties of the heat-transfer gauge and the infra-red signal in this experimental situation (see figure 6). The temperature variation of the

gauge as a function of time for both convective and radiative heating is illustrated in figure 6 (*a*). The onset of the convective heat transfer occurs at the time of shock arrival at the end-wall, while the radiation heat transfer from the hot argon starts later at the ionization time τ_4. Thus, the heat-transfer rate $\dot{q}$ to the gauge has a time dependence

$$\dot{q} = Q_C/\sqrt{t} + Q_R(t-\tau_4), \tag{10}$$

where Q_C and Q_R are constants determined by the convective and radiative heat-transfer rate respectively. The time t is measured from the time of shock

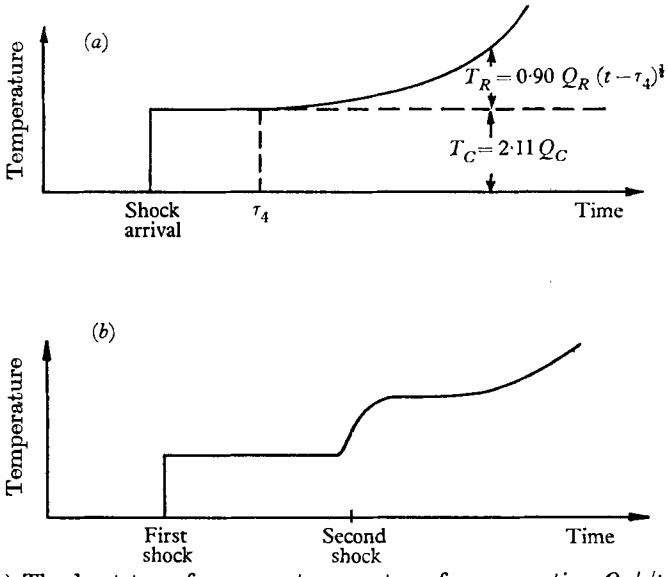

FIGURE 6. (*a*) The heat-transfer-gauge temperature for convective $Q_C/\sqrt{t}$ and radiative $Q_R(t-\tau_4)$ heat inputs. The gauge-temperature $T = 2{\cdot}11Q_C + 0{\cdot}9Q_R(t-\tau_4)^{\frac{3}{2}}$. (*b*) The gauge-temperature variation in a heat-transfer measurement.

arrival at the end-wall. The corresponding temperature rise T of the gauge after a short response time approximates the asymptotic long-time solution (Camac & Feinberg 1962):

$$T = \sqrt{(\pi/k\rho C)}\{Q_C + (\tfrac{4}{3}\pi)\,Q_R(t-\tau_4)^{1{\cdot}5}\} = \{2{\cdot}11Q_C + 0{\cdot}90Q_R(t-\tau_4)^{1{\cdot}5}\}\,^\circ\mathrm{K}. \tag{11}$$

k, ρ, C are the thermal conductivity, density and specific heat of sapphire. For the numerical coefficients, t is in seconds, Q_C in W sec$^{\frac{1}{2}}$/cm^2, and Q_R in W/sec cm^2. Equation (11) shows that the temperature has an instantaneous jump T_C due to the convective heating. The further temperature rise T_R due to the radiation heating can be experimentally separated if it does not rise too sharply.

Figure 6 (*b*) illustrates the experimental measurements. The initial level portion is indicative of only convective heat transfer. After the second rise, radiative heating does become important and makes it difficult to analyse the convective portion. The time between the onset of the first and second rises shown in figure 5 is plotted in figure 7. The curves show the ionization times τ_2 and τ_4 behind the incident and reflected shocks respectively (see equations

(1) and (2)). The time of the second heat pulse is associated with τ_2 and is probably due to a secondary shock produced by the interaction of the reflected shock with the ionization front behind the incident shock, as indicated in figure 1. The rise time of the second level is consistent with an abrupt jump in the heat-transfer input. It should be noted that the ionization process behind the reflected shock occurs during the first level portion and does not change the heat transfer.

The asymptotic solution for the temperature of the back surface given by equation (11) has to be modified for short times when the finite thickness of the

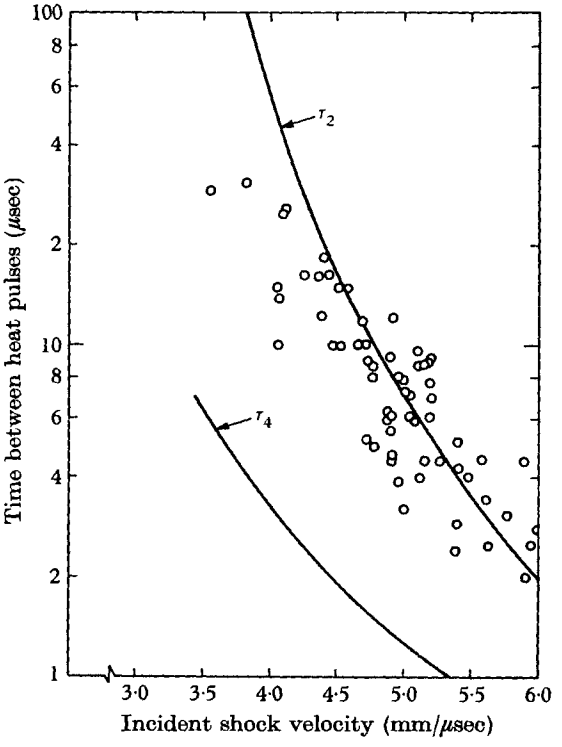

FIGURE 7. The time between the onset of heat transfer and the second rise (see figures 5 and 6). The curves are the ionization times τ_2 and τ_4 behind the incident and reflected shocks respectively.

carbon layer introduces a thermal lag (Camac & Feinberg 1962). For most of the experimental data, the rise time of the heat-transfer signal was approximately 1 μsec as shown in figure 5. Several runs were made in which the experimental rise time was the order of 0·1 μsec, as shown in figure 9, plate 1.

The convective heat-transfer coefficient Q_C for the first level portion is plotted as a function of the incident-shock velocity in figure 8. For all experimental runs, the first portion remains level (within the experimental noise) until the abrupt change to the second level.

The convective heat-transfer rates for the second level were not analysed, because of the large uncertainty due to the radiative heat transfer. There is the

additional complexity of the flow near the wall, which must include a second shock, further ionization relaxation, and radiation cooling.

In order to evaluate the chemical state of the argon behind the reflected shock, the ionization time τ_4 was also determined by measuring the time interval between the onset of (i) the heat-transfer rate to the end-plate, and (ii) the argon continuum emission behind the reflected shock. The end-wall was modified to hold two $\frac{3}{8}$ in. sapphire windows; one was coated with carbon and aluminium for heat-transfer measurements; the other window was clear in order to view

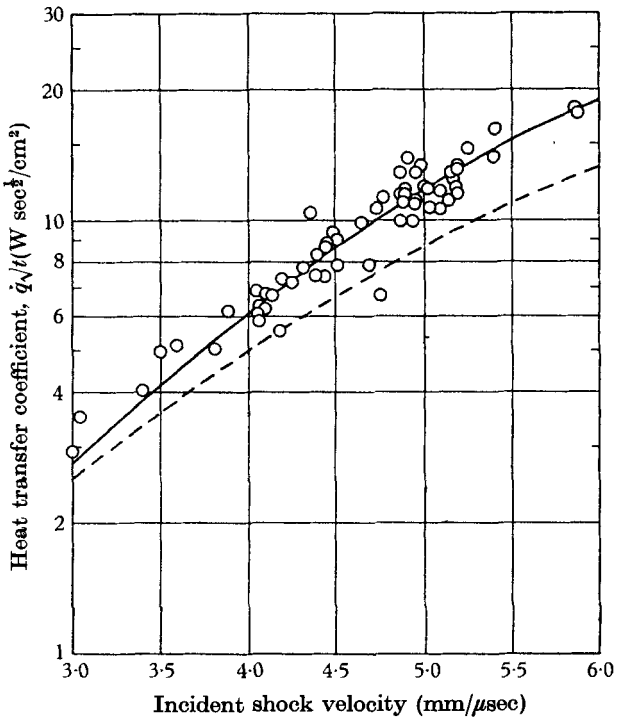

FIGURE 8. The convective-heat-transfer coefficient Q_C for the first level behind the reflected shock. ——, $\gamma = \frac{5}{3}$ for region 2F–4F; – – –, equilibrium boundary layer for region 2F–4E′.

the visible radiation from the argon with a photomultiplier. Experimental runs are shown in figure 9. The onset of heat transfer at the end-plate is precisely the time of shock arrival, while the onset of radiation behind the reflected shock occurs at the ionization-equilibration time τ_4. The experimental measurements of τ_4 are shown in figure 10. The curve, derived from equation (2), shows the ionization times extrapolated from the data of Petschek & Byron (1957).

By comparing figures 7 and 10, one notes that the time τ_4 is less than one-third the time for the onset of the second heat transfer. The experimental heat-transfer rate has the result that the heat-transfer coefficient is essentially independent of the chemical state of the argon behind the reflected shock, i.e. the argon goes from the frozen to the equilibrium-ionization state during the period in which the convective heat-transfer coefficient remains constant.

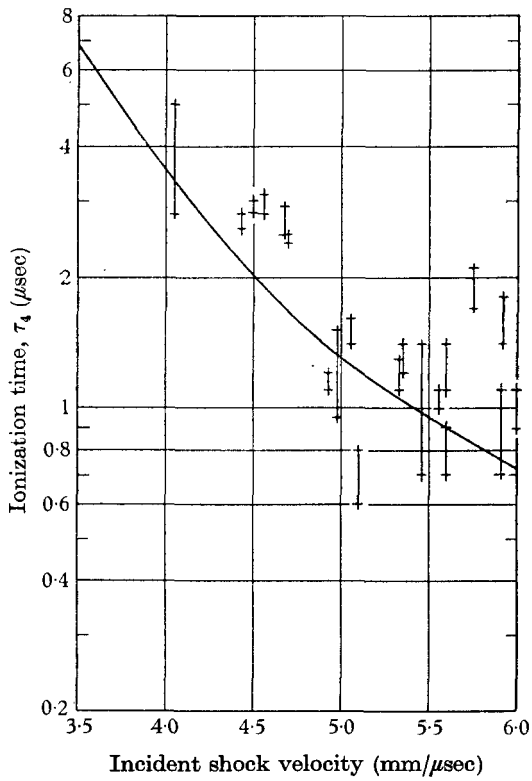

FIGURE 10. Argon-ionization time behind the reflected shock in argon with an initial pressure of 1 mm Hg and temperature of 294 °K. ——, Extrapolated curve from Petschek & Byron (1957).

4. Discussion

The main results reported in this paper are the argon heat-transfer rates to the end-wall. A comparison of our experimental data to theoretical predictions required an evaluation of the state of the argon behind the reflected shock and in the end-wall boundary layer (Camac & Feinberg 1963). The various limiting frozen and equilibrium free-stream conditions are presented in table 1. Actually, the free-stream conditions are complicated by two effects which cause unsteady flow to the end-wall. (i) The effects of end-wall cooling are important during early times, but reduce to a few percent correction after 1 μsec from the time of shock arrival at the end-wall. No correction was applied to the experimental data. (ii) The ionization process causes large changes in the density, temperature, and reflected-shock velocity. Heat-transfer measurements were made during the transition from the frozen to the equilibrium-ionization conditions. The flow-field and ionization conditions of Camac & Teare (1964) were used in the theoretical analysis of the heat-transfer rates.

Figure 8 shows the main experimental results of the present investigation. The circles represent the heat-transfer coefficient measured with the infra-red gauge. Prior to the gas-ionization time τ_4 behind the reflected shock the heat

transfer was predominantly from neutral argon, since both the inviscid flow and the boundary layer had not had time to ionize.

The neutral argon measurements are compared to the perfect-gas ($\gamma = \frac{5}{3}$) heat-transfer calculations of Fay & Kemp (1965), who give an analytic formula for the convective-heat-transfer coefficient Q_C:

$$Q_C = 0{\cdot}80 T_e \sqrt{\left\{\left(\frac{C_p \rho_e k_e}{\nu(\nu+1)}\right)(1-(\nu+1)(T_w/T_e)^{\nu}+\nu(T_w/T_e)^{\nu+1})\right\}}. \tag{12}$$

T_e, k_e and ρ_e are the temperature, heat conductivity and density in the external free stream. T_w is the gauge temperature, that is the room temperature plus the temperature rise of the gauge. The *only* transport property required in the theory

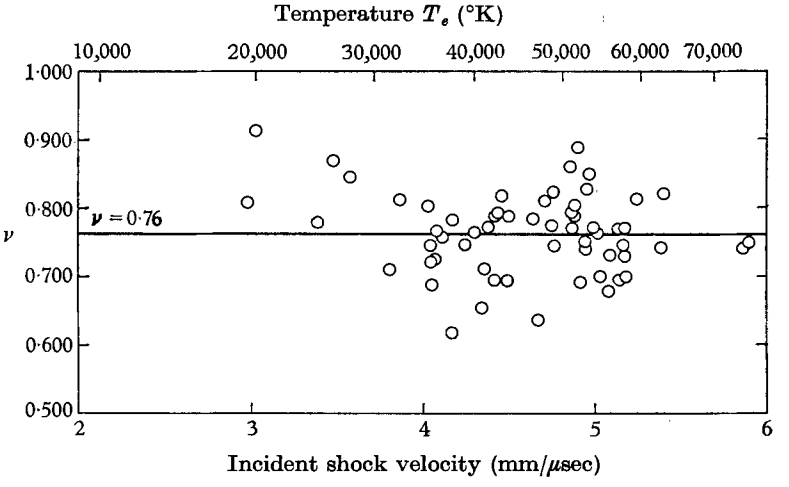

FIGURE 11. The experimental determination of the exponent ν, assuming a power-law temperature dependence T^{ν} for the neutral-argon thermal conductivity.

was the thermal conductivity of neutral argon, k, which was assumed to have a power-law temperature variation T^{ν}, where ν is a constant. The solid line in figure 8 shows the results of the theory for $\nu = 0{\cdot}75$, determined by Amdur & Mason (1958) over the temperature range from 1500 to 15,000 °K.

Figure 11 shows an analysis of the data in terms of ν, assuming

$$k = 4{\cdot}2 \times 10^{-5}(T/300)^{\nu} \text{ cal/sec cm °K}.$$

A value for ν was obtained for each experimental run by inserting the computed free-stream conditions k_e, ρ_e and T_e, and the measured value of T_w and Q_C in (12) and solving for ν. A least-square fit to the data gives $\nu = 0{\cdot}76 \pm 0{\cdot}03$ (probable error) over the free-stream temperature range from 20,000 to 75,000 °K. This value of ν is in excellent agreement with the work of Amdur & Mason (1958) and can be interpreted as experimental confirmation of $T^{\frac{3}{4}}$ up to 75,000 °K.

In each experimental run, the heat-transfer coefficient remained constant during and after the ionization process until the arrival of the second shock. This can be qualitatively explained (Fay & Kemp 1965) by noting that the thermal conductivity of neutral argon at the initial frozen temperature of about 70,000 °K is essentially that for electrons at the final equilibrium temperature of 15,000 °K.

A theoretical comparison was also made with the measurements after the free stream reached equilibrium ionization. The unsteady-flow solutions (Camac & Teare 1964) (2F–4E′) were used for the free-stream conditions, see table 2. The dashed curve in figure 8 shows the equilibrium-boundary-layer solutions of Fay & Kemp (1965). The theoretically-predicted heat-transfer rate is 20–30 % below the measured values. There are several possible reasons for the discrepancy between theory and measurements. The time interval between the ionization time τ_4 and the end of the first level heat transfer is approximately $3\tau_4$ and may be too short for establishing the new conditions throughout the boundary layer. Also, the state of the gas at the edge of the boundary layer during and after the ionization relaxation is quite difficult to determine, and the simplified method (Camac & Teare 1964) used may introduce some error. The deviation from the similarity boundary-layer solution (Fay & Kemp 1965) during the transition to equilibrium ionization was not estimated. Finally, the equilibrium theory does not include the effects of different electron and ion temperatures. Thus, it is felt that, with these possible sources of errors, the theory and experiment are in substantial agreement.

The argon-ionization time behind the reflected shock was also measured (see figure 10). Our results are in agreement with an extrapolation of the incident-shock measurements of Petschek & Byron (1957) to conditions behind the reflected shock.

This work was supported jointly by Headquarters, Ballistic Systems Division, Air Force Systems Command, United States Air Force under Contract AF 04(694)-414, and Air Force Office of Scientific Research, Office of Aerospace Research, United States Air Force under Contract AF 49(638)-1129.

REFERENCES

Amdur, I. & Mason, E. A. 1958 *Phys. Fluids*, **1**, 370.

Bershader, D. & Rutowski, R. W. 1961 *ARS Paper*, no. 1998-61.

Byron, S. & Rott, N. 1961 *Proc.* 1961 *Heat-Transfer and Fluid-Mech. Inst.*, ed. R. C. Binder *et al.* Stanford University Press.

Camac, M. & Feinberg, R. M. 1962 *Rev. Sci. Instrum.* **33**, 964.

Camac, M. & Feinberg, R. M. 1963 *Avco-Everett Res. Lab., Res. Rep.* no. 168.

Camac, M. & Kemp, N. H. 1963 *AIAA Paper*, no. 63-460.

Camac, M. & Teare, J. D. 1964 *Avco-Everett Res. Lab., Res. Rep.*, no. 183.

Fay, J. A. 1964 *The High Temperature Aspects of Hypersonic Flow*, p. 583, ed. W. C. Nelson. London: Pergamon Press.

Fay, J. A. & Kemp, N. H. 1965 *J. Fluid Mech.* **21**, 659.

Goldsworthy, F. A. 1959 *J. Fluid Mech.* **5**, 164.

Jukes, J. 1956 *Master of Aeronautical Engineering Thesis, Cornell Univ.*

Mies, F. H. 1962 *J. Chem. Phys.* **37**, 1101.

Petschek, H. E. & Byron, S. 1957 *Ann. Phys.* **1**, 270.

Petschek, H. E., Rose, P. H., Glick, H. S., Kane, A. & Kantrowitz, A. R. 1955 *J. Appl. Phys.* **26**, 83.

Reilly, J. P. 1963 *Master of Aeronautical Engineering Thesis, Mass. Inst. Tech.*

Smiley, E. F. 1957 *Ph.D. Thesis, The Catholic Univ. America.*

Sturtevant, B. 1964 *APS Bull.* **9**, 583.

Van der Noordaa, R. S. L. 1957 *Master of Aeronautical Engineering Thesis, Cornell Univ.*